GR Final Project
Visualizing Spacetime around Black Holes and Neutron Stars

Devanshu Panchal (dp29958) and Patrick Rall (pr22842)

May 4, 2018

1   Introduction

Neutron stars are a final stage in the lifetime of massive stars. They are relativistic objects with a strong gravitational field. Just like black holes, the curvature of spacetime around a neutron star can be visualized using gravitational ray-tracing techniques. In this project, we visualize the warped spacetime around a various black holes and a particular model of neutron star spacetime. We study the shadows that these objects cast, as well as gravitational lensing of a light source behind the objects. To do this, we developed ray-tracing software to compute the evolution of null geodesics on an arbitrary curved metric. Images from well-studied black hole metrics [1, 2, 3] show that our protocol produces reasonable results. We find that the paths of null geodesics around a spinning neutron star are strongly impacted by frame dragging. We also observe a phenomenon where light appears to 'bounce' off the neutron star, causing mirages of the surrounding sky to appear on its surface.

2   Motivation

In 1918, Einstein published his geometric theory of gravity [4]. The General Theory of Relativity redefined the force of gravity as the effect of the curvature and the bending of spacetime. According to this theory, each particle world line is a geodesic of the 4D geometry. The equation of a geodesic in General Relativity governs the evolution of the particle's 3D trajectory as a function of time. A measure of intrinsic curvature in this theory is the Riemann tensor ($R^{\alpha}{}_{\beta\gamma\delta}$). This tensor encodes the local curvature of spacetime through second derivatives of the metric ($g_{\mu\nu}$). Given the metric for the spacetime around a massive body, one could visualize the 4D spacetime curvature as perceived by an observer. A technique used to visualize the spacetime curvature is the gravitational analog of optical ray-tracing, which is used in computer graphics to visualize scenes involving mirrors and lenses. The technique employs tracing the null geodesics of light around a massive body. Ray-tracing was one of the techniques employed by the film-makers of the science-fiction movie Interstellar to visualize the accretion disk around a black hole [5]

The goal of this project is to visualize the curved spacetime around a neutron star using ray-tracing techniques. Neutron stars are fascinating objects: a neutron star is the collapsed core of a massive star, with mass densities comparable to the average atomic density and gravitational effects comparable to those around a black hole. Owing to the nonlinearity of the Einstein Field Equations, deriving an all-purpose metric of a neutron star is difficult. Theorists have to rely on existing, solvable solutions of curved spacetime metric to develop an approximate metric for a neutron star. We plan to study the metric first introduced by Kostas Glampedakis and Stanislav Babak [6].

We wrote a Python application that calculates the evolution of geodesics from from a camera placed in front of the neutron star, exploiting time-reversal symmetry to justify using the camera as a source of the geodesics. We will test these scripts by ray-tracing the Schwarzschild, Kerr, and Reissner–Nordström [1, 2, 3] black hole metrics. Although the Python language is not very fast, its computer algebra library SYMPY permits automatic evaluation of the complicated algebra needed to get from an input metric to fast evaluation of the geodesic equation.

The rest of the document is organized as follows: Section 3 gives a brief overview of the theory behind neutron stars, geodesic equation, and the black hole and neutron star metrics. Section 4 describes the

development of the code for ray-tracing and calculation of the variables. Section 5 discusses the ray-tracing for the three black hole and the neutron star metric. Section 6 gives a brief overview of the project with some concluding remarks.

3   Theoretical Background

Typically, neutron stars have a radius of 10 km and mass in the range of 1.4–3 $M_\odot$. Any star whose mass is greater than 8 $M_\odot$ has the potential to evolve into a neutron star. When a star the size of 8 $M_\odot$ burns out all the nuclear fuel in its core, the thermal pressure cannot balance out the inward-pointing gravitational pressure. The gravitational pressure causes the star to implode, overcoming the electron-degeneracy pressure. As the star further implodes, the electrons and the protons combine to form neutrons via electron capture, releasing a flood of neutrinos. When nearing nuclear densities, the inward collapse halts. The in-falling outer envelope is flung outwards by the flux of neutrinos produced in the electron capture process. The star goes supernova, leaving behind a star composed solely of neutrons—a neutron star.

As a star collapses, its rotation speed increases to conserve angular momentum. Hence, newly formed neutron stars have a rotational speed on the order of several hundred hertz. Therefore, matter at the equator of the neutron stars rotate with linear speeds comparable to the speed of light (c). Neutron stars are also very dense because of their matter concentration. Observed densities of neutron stars can range from 3.7×10^{17} to 5.9×10^{19} $\mathrm{kg\,m^{-3}}$—comparable to atomic density. Small radius and high density lead to strong gravitational acceleration on the surface of the star. Strong gravitational fields acts as a gravitational lens, bending light rays like an ordinary optical lens would bend rays of light. However, since neutron stars aren't as massive as black holes, the effect of gravitational lensing is small compared to ones expected to be seen around a black hole. The high mass densities and strong gravitational fields can be approximated using black hole metrics.

One must perform complex relativistic hydrodynamical calculations to obtain an exact metric for a neutron star. Since neutron stars are relativistic objects, their structure and evolution needs to be studied using General Theory of Relativity. A compactness parameter that conveys the importance of relativistic corrections is used. The compactness parameter is defined as the ratio of the Schwarzschild radius (r_g) to the radius of the star (R). For a typical neutron star, the compactness is 0.2–0.4, for all other stars the ratio is much less than one. Therefore, neutron stars are closer to a black hole than to a regular star in a solar system.

3.1   Geodesic Equation

Consider a force-free particle in free space. A particle is said to be force-free if the particle moves at a constant velocity, i.e.,

$$\frac{d^2 x^\mu}{d\tau^2} = 0 \tag{1}$$

Here, x^μ is the particle's position and τ is the proper time. The equation above describes acceleration in the frame of the moving particle. If we want to describe the acceleration in any frame, we use the transformation

$$g_{\mu\nu} = \frac{\partial \tilde{x}^\alpha}{\partial x^\mu} \frac{\partial \tilde{x}^\beta}{\partial x^\nu} \eta^{\alpha\beta} \tag{2}$$

Here $g_{\mu\nu}$ is the metric for curved spacetime and $\eta_{\alpha\beta}$ is the Minkowski metric. We can rewrite Eq. 1 as

$$\frac{d^2 x^\mu}{d\tau^2} + \Gamma^\mu{}_{\nu\rho} \frac{dx^\nu}{d\tau} \frac{dx^\rho}{d\tau} = 0 \tag{3}$$

Where $\Gamma^\mu{}_{\nu\rho}$ are the affine connections, called the Christoffel symbols. The Christoffel symbols are defined in terms of the metric components as

$$\Gamma^\gamma{}_{\mu\nu} = \frac{1}{2} g^{\gamma\alpha} \left(g_{\alpha\nu,\mu} + g_{\alpha\mu,\nu} - g_{\mu\nu,\alpha} \right) \tag{4}$$

Here, $g_{\alpha\nu,\mu}$ is the derivative of the metric $g_{\alpha\nu}$ in the component μ. By definition, the Christoffel symbol is symmetric in its last two indices, i.e., $\Gamma^\gamma{}_{\mu\nu} = \Gamma^\gamma{}_{\nu\mu}$. Equation 3 is called the Geodesic equation. It describes the motion of free particles in a spacetime with arbitrary coordinates.

The geodesic equation can be used to calculate the deflection of a light beam in presence of a strong gravitational field (even though the notion of proper time is not meaningful for light). In fact, one of the first experiments to prove the General Theory of Relativity was based on the deflection of light coming from distant stars in presence of the gravitational field of our Sun [7].

3.2 Einstein Field Equations

The curved spacetime metric and the geodesic equation are enough to perform ray-tracing to visualize the spacetime. The Einstein Field Equations are a set of second-order differential equations given by [8]

$$R_{\mu\nu} - \frac{1}{2}Rg_{\mu\nu} = \frac{8\pi G}{c^4}T_{\mu\nu}. \tag{5}$$

Here, $R_{\mu\nu}$ is the Ricci tensor, G is the universal gravitational constant, R is the Ricci scalar, and $T_{\mu\nu}$ is the stress-energy tensor. In this project we set $G = c = 1$ to simplify calculations so we can focus on creating interesting images. However, this means that the images we create do not necessarily correspond to what a real-life observer would see. This choice is standard among previous ray-tracing studies [5, 9, 10]

3.3 Black Hole and Neutron Star Metrics

Karl Schwarzschild was the first one to find the solution of the Field Equations for a stationary, spherically-symmetric body [1]. The Schwarzschild metric for a static, uncharged, non-rotating black hole is [11]

$$ds^2 = -\left(1 - \frac{r}{r_s}\right)c^2dt^2 + \frac{1}{1 - \frac{r}{r_s}}dr^2 + r^2(d\theta^2 + \sin^2(\theta)d\phi^2), \tag{6}$$

where c is the speed of light and r_s is the Schwarzschild radius defined by

$$r_s = \frac{2GM}{c^2}. \tag{7}$$

G represents the universal gravitational constant and M representing the mass of the object. The Schwarzschild radius for a black hole is also called the event horizon. An event horizon is a boundary around a black hole beyond which no particle, not even light can escape. Thus, if a light ray were to cross the event horizon, it would never escape and will be "pulled" to the center of the black hole.

Reissner and Nordström were the first to solve for a static, charged, non-rotating black hole [3]. The Reissner–Nordström metric is

$$ds^2 = \left(1 - \frac{r_s}{r} + \frac{r_Q^2}{r^2}\right)c^2dt^2 + \left(1 - \frac{r_s}{r} + \frac{r_Q^2}{r^2}\right)^{-1}dr^2 + r^2d\theta^2 + r^2sin^2\theta d\phi^2. \tag{8}$$

Here, r_Q is a length scale given by

$$r_Q^2 = \frac{Q^2G}{4\pi\epsilon_0 c^4}. \tag{9}$$

Since photons have no charge, we expect Reissner–Nordström ray-tracing to be similar to Schwarzchild ray-tracing.

The Kerr solution to the Einstein Field Equations represents an empty spacetime around an uncharged, rotating black hole. The metric in Boyer–Lindquist co-ordinates is [11]

$$ds^2 = -\left(1 - \frac{rr_s}{\Sigma}\right)c^2dt^2 + \frac{\Sigma}{\Delta}dr^2 + \Sigma d\theta^2 + \left(r^2 + a^2 + \frac{rr_sa^2}{\Sigma}\sin^2\theta\right)\sin^2\theta d\phi^2 - \frac{2rr_sa\sin^2\theta}{\Sigma}cdtd\phi. \tag{10}$$

Here, r_s is the Schwarzschild radius, a, Σ, and Δ are length scales defined as

$$a = \frac{J}{Mc} \tag{11}$$

$$\Sigma = r^2 + a^2\cos^2\theta \tag{12}$$

$$\Delta = r^2 - rr_s + a^2 \tag{13}$$

3

The Kerr black hole has four notable surfaces: two when the g_{rr} term diverges and the two when g_{tt} term diverges. These occur at the radii:

$$r_\Delta = \frac{1}{2}\left(r_s \pm \sqrt{r_s^2 - 4a^2}\right) \tag{14}$$

$$r_\Sigma = \frac{1}{2}\left(r_s \pm \sqrt{r_s^2 - 4a^2 cos^2\theta}\right) \tag{15}$$

The outer r_Δ singularity is an event horizon: a point of no return. The r_Σ singularities mark the ergosphere, a region with extreme frame dragging. Since the inner r_Σ solution is contained within the event horizon, only the outer solution is important for our purposes [12].

The presence the cross term $cdtd\phi$ in the Kerr metric implies the mixing time and the azimuthal angle (ϕ) co-ordinates. The cross term in the metric gives rise to the phenomenon of frame dragging—a general relativistic phenomenon which drags inertial frames because of the rotation of nearby matter. To understand frame dragging in simpler terms, let us consider a freely-falling photon directed towards the center of a Kerr black hole. If the black hole were not rotating, the photon would fall directly into the black hole. However, because the black hole and the spacetime around the black hole are rotating, the photon does not fall straight: the photon is imparted an angular momentum and is dragged around the black hole.

The neutron star metric we use in this project is the one first proposed by Glampedakis and Babak [6]. They assumed the metric was not exactly a Kerr metric, but deviates slightly from the Kerr metric:

$$g_{\mu\nu} = g_{\mu\nu}^K + \epsilon h_{\mu\nu}. \tag{16}$$

Here, $g_{\mu\nu}^K$ is the Kerr metric, ϵ is the perturbation parameter and $h_{\mu\nu}$ is a metric with components given by

$$h_{tt} = \left(1 - \frac{2M}{r}\right)^{-1}[(1 - 3\cos^2\theta)\mathcal{F}_1(r)] \tag{17}$$

$$h_{rr} = \left(1 - \frac{2M}{r}\right)^{-1}[(1 - 3\cos^2\theta)\mathcal{F}_1(r)] \tag{18}$$

$$h_{\theta\theta} = -\frac{1}{r^2}[(1 - 3\cos^2\theta)\mathcal{F}_2(r)] \tag{19}$$

$$h_{\phi\phi} = -\frac{1}{r^2\sin^2\theta}[(1 - 3\cos^2\theta)\mathcal{F}_2(r)] \tag{20}$$

The functions $\mathcal{F}_1(r)$, $\mathcal{F}_2(r)$ are defined as

$$\mathcal{F}_1(r) = -\frac{5(r - M)}{8Mr(r - 2M)}(2M^2 + 6Mr - 3r^2) - \frac{15r(r - 2M)}{16M^2}\ln\left(\frac{r}{r - 2M}\right) \tag{21}$$

$$\mathcal{F}_2(r) = -\frac{5}{8Mr}(2M^2 - 3Mr - 3r^2) + \frac{15}{16M^2}(r^2 - 2M^2)\ln\left(\frac{r}{r - 2M}\right) \tag{22}$$

Since the Glampedakis–Babar metric is derived as a quasi-Kerr solution for neutron stars, we will assume that the event horizons for the Glampedakis–Babar metric are the ones for the Kerr metric. An interesting property of the Kerr event horizons is the sign reversal of the g_{tt} term if one were to fall within the outer horizon into to ergosphere. In the ergosphere, any object, massless or not has to rotate faster than light to not co-move with the spacetime. Another interesting phenomenon is the possibility of negative energy for a particle in the ergosphere. Negative energy may sound unphysical, but since the time coordinate changes sign in the ergosphere, a particle having negative energy can lead to interesting results. The Penrose process is where a particle falls into the ergosphere and is split into two—a negative energy and a positive energy particle. The negative energy particle falls into the black hole and the positive energy particle escapes the ergosphere with more energy than it had at the beginning. It may not be naïve to assume that the Penrose process creates energy out of nothing. However, when the positive energy particle escapes the ergosphere, it slows down the rotation of the black hole, thereby conserving energy. Although the Penrose process is hypothetical and will not be seen in our visualizations, it is an interesting aspect of rotating black holes.

The next section will outline our ray-tracing program and how the code works. To test the program, we will use the Schwarzschild and the Reissner–Nordström metrics. Once we test the code on static metrics, we will run the program for the Kerr and the Glampedakis–Babar metric.

4   Procedure

We wrote a Python application that integrates the geodesic equation for multiple input metrics. The software supports 'ray diagrams' showing the motion of light in the XY-plane, as well as 'camera images' rendered using a virtual piece of film. Many measures were taken to make this software run as efficiently as possible, so despite Python not being a particularly fast language all diagrams in this report took less than half an hour to render.

For more complicated metrics, evaluating the Christoffel symbols is intractable to do by hand. The SYMPY library features a computer-algebra system permitting automatic computation of derivatives (among many other things). Thus, we only had to enter the metric into the software, and the Christoffel symbols are automatically generated. Furthermore, SYMPY permits 'baking' an expression into a quick-to-evaluate lambda function, which is critical for our application since the geodesic equation must be evaluated very many times. For complicated metrics, calculating the derivatives and baking the lambda function actually took longer than the ray-tracing. In particular, the neutron star metric took about half an hour to bake. Fortunately, one can use the PICKLE and DILL python libraries to serialize a lambda expression and store it on disk. Using this trick we only had to bake each metric once. All of our metrics have parameters, e.g. M, J, Q, ϵ, so our lambda functions actually use currying to yield a function of only $x^\mu, dx^\mu/d\tau$ after parameters are specified. This made complicated diagrams that loop or animate over charges Q or angular momenta J possible. We perform ray-tracing in parallel.

To generate images of the black hole or neutron star, we simulate a virtual camera (see Figure 1). Ray-tracing begins at the focal point of the camera at $x^\mu = (0, 7M, 0, 0)$. A camera film of width and height $3M$ in the ZY plane is centered on the X-axis one focal length $f = 1M$ away from the focal point. For every pixel on the film, the spatial 3-vector from the point on the film to the focal point is computed. This vector is normalized to a unit vector, and then used as the spacial component of $dx^\mu/d\tau$, with $dx^0/d\tau = 1$. In addition to generating images, we also generate 'ray diagrams' by recording the position of the ray at every time step and projecting the 4-vector into the XY plane.
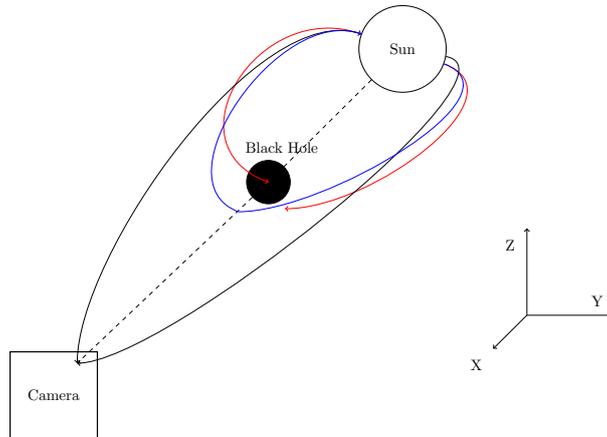
Figure 1: Camera setup. Exploiting time-reversal symmetry, ray-tracing is performed in reverse starting at the focal point. For each pixel, the vector from the pixel to the focal point is computed. This vector is normalized and set as the initial velocity vector. To illustrate, rays painted red are the ones which fall into the black hole. The rays painted gray are the ones which escape the black hole and the ones painted blue are those take a U turn. The blue rays will be rare, the ones which get deflected the most because of the curvature around a black hole. Future diagrams use a different color scheme.

The color of the pixel is determined by where the ray terminates. We terminate a ray if it enters the event horizon, or if a ray has $x^r > 8M$ and is considered 'escaped.' To gain a better sense of the space, we color the celestial sphere in a checkerboard pattern by looking at x^θ and x^ϕ, Figure 2. We also use this technique to render images of gravitational lensing by marking a target at the back of the celestial sphere in a different color.

Since we did not use a pre-written numerical integration package, we had to solve some minor numerical issues ourselves. In particular, the integration rate needed to be adjusted as a function of location.

This is due to either the spherical coordinate system (e.g. near the Z-axis), or regions of spacetime with extreme curvature (e.g. inside the ergosphere of a Kerr black hole). For the neutron star, it was difficult to determine exactly what regions needed higher integration rates, so we inspected the value of $d^2x^\mu/d\tau^2$ and adjusted the step size until the distance moved was below a threshold. If the step size is too large, visual artifacts occur like the 'notches' in Figure 3 in the Schwarzschild black hole. But for more complicated metrics it may be difficult to tell what features are artifacts and what features are physical. In some ways this problem is unavoidable, but we mitigated the problem by looking at previous literature and experimenting with different integration rates to see which features are stable.
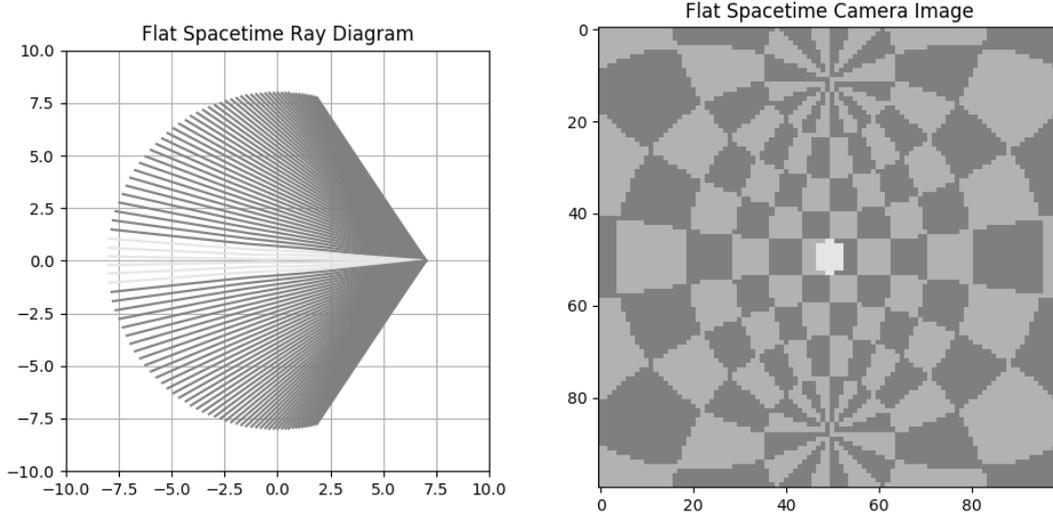
Figure 2: Ray-tracing in flat spacetime. A celestial sphere of radius $8M$ is colored in a checkerboard pattern. To study lensing, we sometimes mark a $4M$ wide patch at the back of the sphere in a bright color.
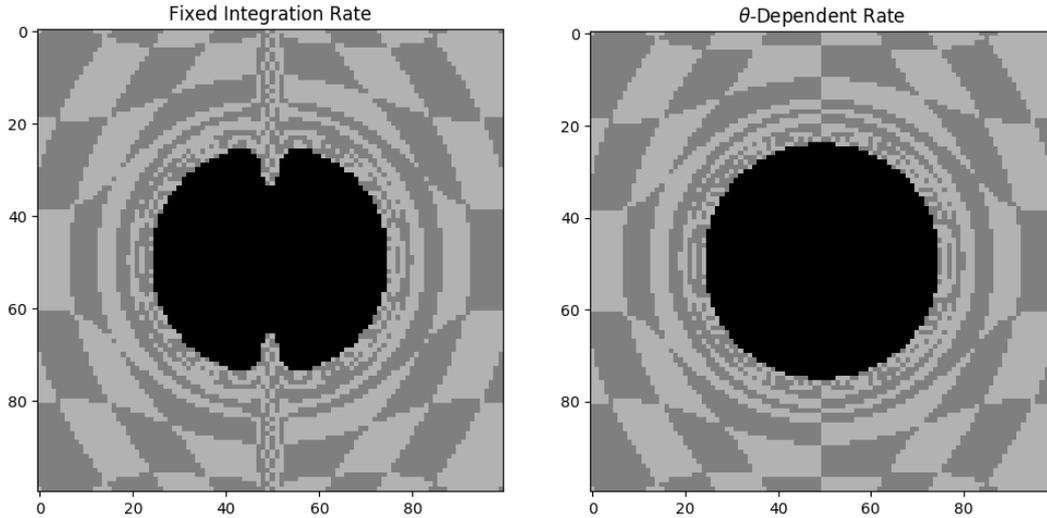
Figure 3: Images with the Schwarzschild metric (without the bright patch). Left: the step size is constant at 0.05. As rays pass close to the z axis, the small values of θ cause errors in numerical integration. Right: errors are removed if step size is reduced.

We did not expect our images to look as beautiful as the renderings in the movie Interstellar. However, we can still replicate the physics behind the appearance of an accretion disk around a black hole. To do this, we terminated rays that entered a wedge with $|x^\theta - \pi/2| < 0.05$ and $x^r < 5M$, and colored these rays white. We see that rays that travel above the black hole are bent around to collide with the accretion disk, causing bands to appear above and below the black hole (see Fig. 4). This is visually similar to the images in Interstellar 4.
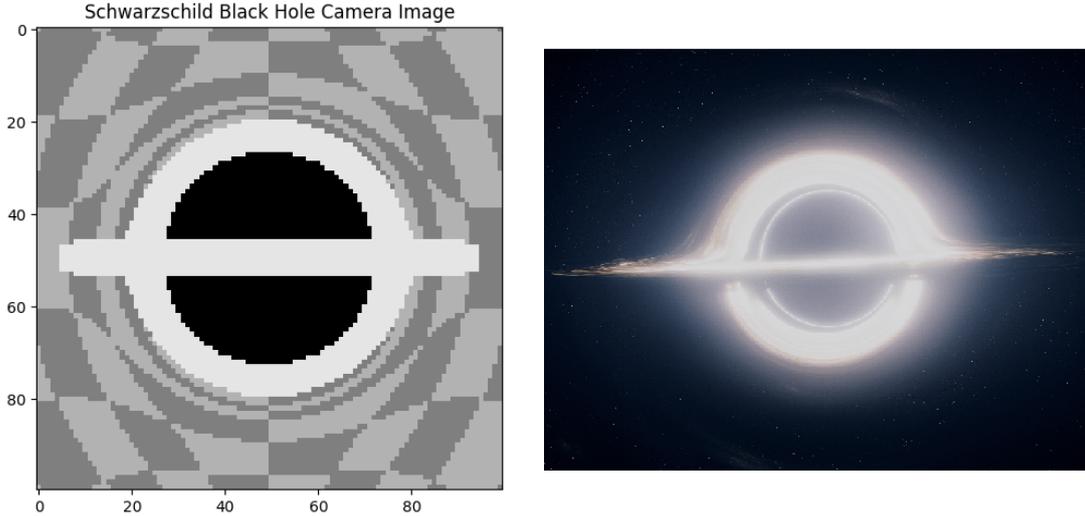
Figure 4: Left: A Schwarzschild black hole with an accretion disk, as rendered by our software. Right: the black hole as seen in the move Interstellar. (Image source: wired.com)

5 Results

In this section we discuss the four different metrics implemented in our software. Our primary points of interest are the shadow cast by the black hole and gravitational lensing. The Schwarzschild and Reissner–Nordström metrics produce standard results, so our code seems to be working correctly. The rotating black hole and neutron star look much more interesting. For all of our metrics we choose $M = 1$.

5.1 Schwarzschild Black Hole

Our software produces familiar images for gravitational lensing Fig. 5 for the Schwarzschild metric. When the bright patch is centered on the X axis (see Fig. 2) we see that the light is bent around in a circle. We experiment with different positions of the bright patch to observe different shapes.

The patch is rather small in Fig. 2, but appears much larger in size in Schwarzschild spacetime. The ray diagram in Fig. 5 offers an explanation: Taking a different path around the black hole causes multiple rays to hit the same point on the bright patch, effectively re-using it to cast more light.

We also observe that some beams of light that pass very close to the black hole are deflected so strongly that they do a U-turn. This explains why the sky close to the black hole looks jumbled.

5.2 Reissner–Nordström Black Hole

For a charged black hole we utilize the Reissner–Nordström metric, which has a charge parameter $Q \leq M$. The gravitational lensing looks pretty much the same as the Schwarzschild black hole. The shadow of the object has become smaller, since the event horizon is now $M + \sqrt{M^2 - Q^2} \leq 2M$. In Fig. 6 we show a Reissner–Nordström black hole with $Q = 0.9$. If the test particles were charged, there would be an additional force causing the paths to be quite different.
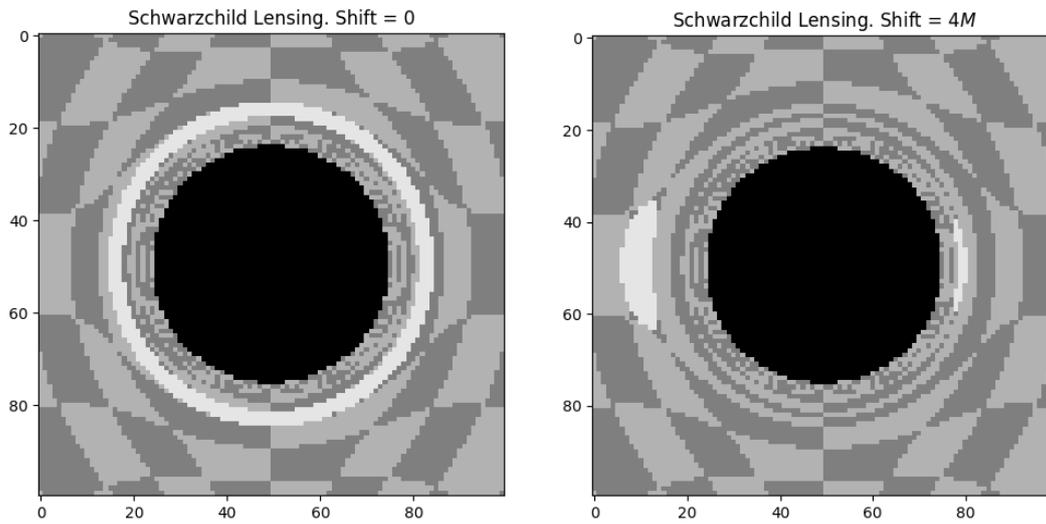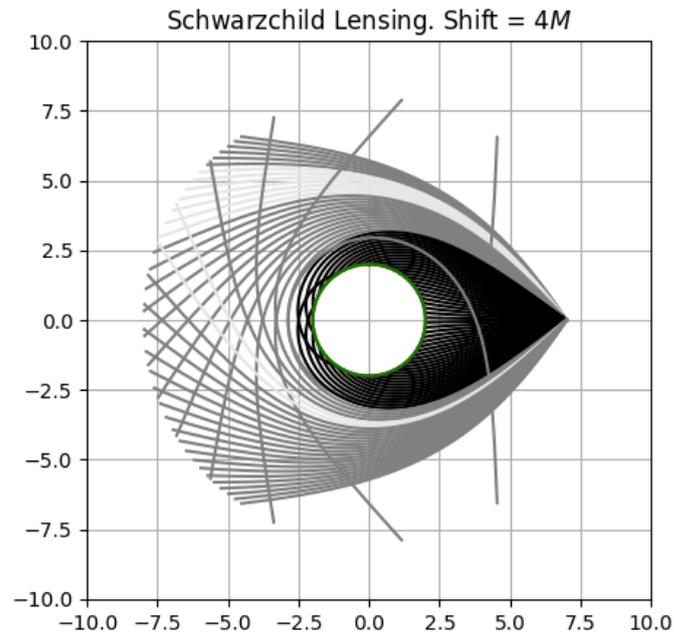
Figure 5: Gravitational lensing for the Schwarzschild metric. The bright patch behind the black hole is shifted along the Y axis.
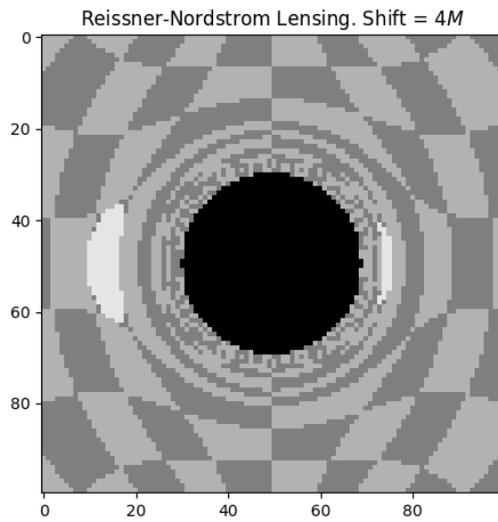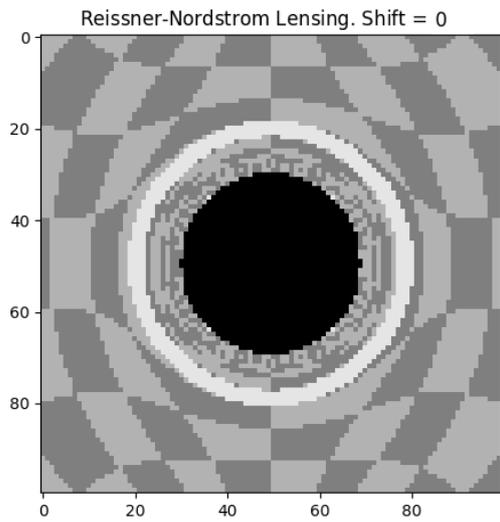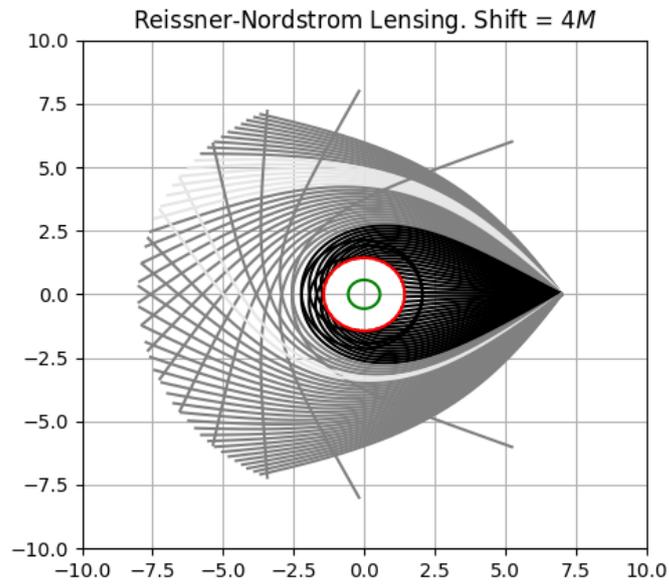
Figure 6: Gravitational lensing for the Reissner-Nordström black hole metric with $Q = 0.9$. In the ray diagram, the event horizon is shown in red and the Cauchy horizon is shown in green. The Cauchy horizon does not affect ray-tracing.
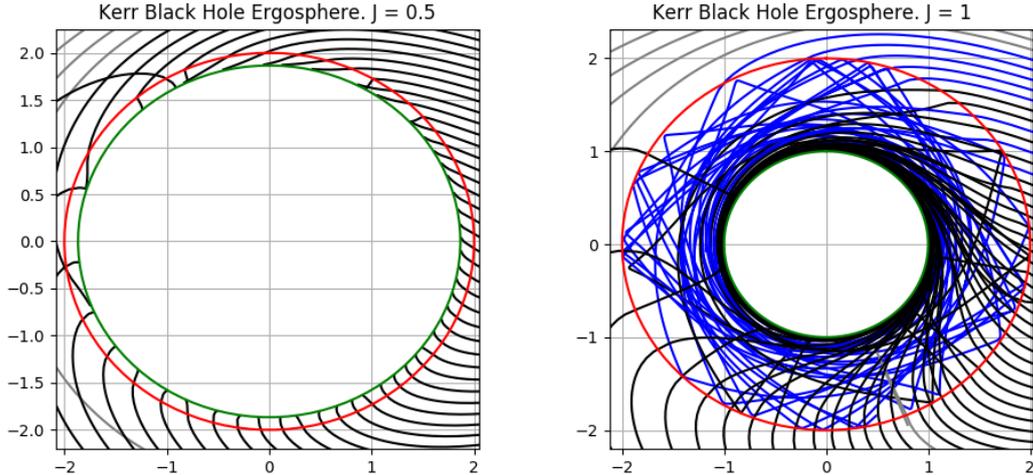
Figure 7: Close-up of a ray diagram in the ergosphere of a Kerr black hole for $J = 0.5$ and $J = 1$. Rays that exceed 100000 steps are terminated and highlighted blue. Despite significantly reduced step size some rays appear to not co-rotate. Rays entering the ergosphere at shallower angles seem to orbit the black hole for longer.

5.3 Kerr Black Hole

The Kerr metric describes a rotating black hole with a charge parameter J. It is also often described with a parameter $a = J/Mc$ but since we choose $c = M = 1$ we have $J = a$. The Kerr black hole spacetime is interesting because it exhibits frame dragging: light that co-rotates with the black hole moves faster according to an external observer. This causes the shape of the ray paths to become severely asymmetrical.

To understand where to terminate rays we must study the Kerr black hole's important surfaces. We found the surfaces $r_\Delta = \frac{1}{2}\left(r_s + \sqrt{r_s^2 - 4a^2}\right)$ and $r_\Sigma = \frac{1}{2}\left(r_s + \sqrt{r_s^2 - 4a^2\cos^2\theta}\right)$ most relevant. r_Δ is the event horizon and point of no return, and the obvious termination point for beams of light. r_Σ marks the outer boundary of the ergosphere. Inside the ergosphere frame dragging becomes so severe that particles must travel faster than the speed of light to not co-rotate with the black hole. Inside this region numerical integration becomes unstable, even after significantly decreasing the integration step size (see Fig 7).

As visible in Fig. 7, many rays exhibit reasonable frame dragging behavior. But despite the very low step size some rays do not co-rotate (which is unphysical), or appear to move in straight lines which suggests the integration is not working correctly. At the very least, although escape from the ergosphere is possible in principle it does not seem to occur in this situation. This justifies the choice to terminate the ray-tracing in the ergosphere.

In Fig. 8 we show a ray diagram as well as the shadows and gravitational lensing in the Kerr metric. We do not vary the position of the bright patch since we found that there is no interesting change. Although the bright patch is directly behind the black hole, the patch is not visible above or below. The frame dragging visible in the ray diagram has reduced the left part of the patch to a small point, whereas the right patch looks more similar to the Schwarzschild black hole lensing.

The shadows of a Kerr black hole have been previously studied, and our results appear to match these results (see Fig. 8). When $J = a = 1$, there is a clearly visible 'notch' on the left side of the black hole that does not appear to be an artifact from numerical integration. Interestingly, a work that numerically fits Dürer–Pascal Limaçons [13] to the shadows of Kerr black holes does not see the notch for $a = 1$. But these Limaçons are perfectly capable of describing such notches, most famously in the special case of the cardioid.
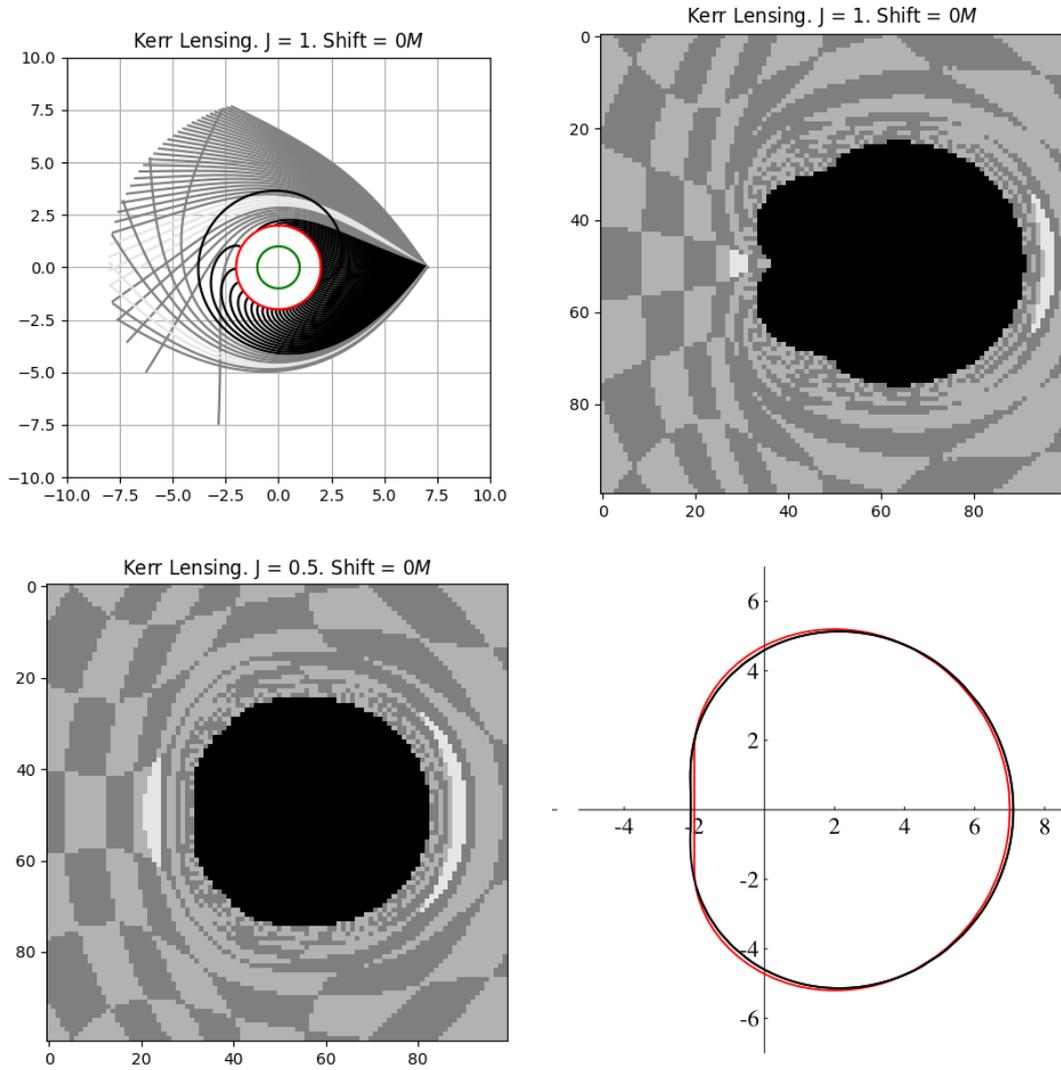
Figure 8: Gravitational lensing for the Kerr black hole metric for different values of J. Since rays that enter the ergosphere tend to eventually fall into the black hole, we terminate the rays at the ergosurface for this figure. The ray diagram shows the effects of frame dragging, as well as the outer boundary of the ergosphere in red. The patch of light is significantly less visible in this metric, but the shadow of the black hole develops an oblong shape. The shape can be approximated using Dürer–Pascal limaçons, as shown by a figure adapted from [13] (with $a = 1$).

11
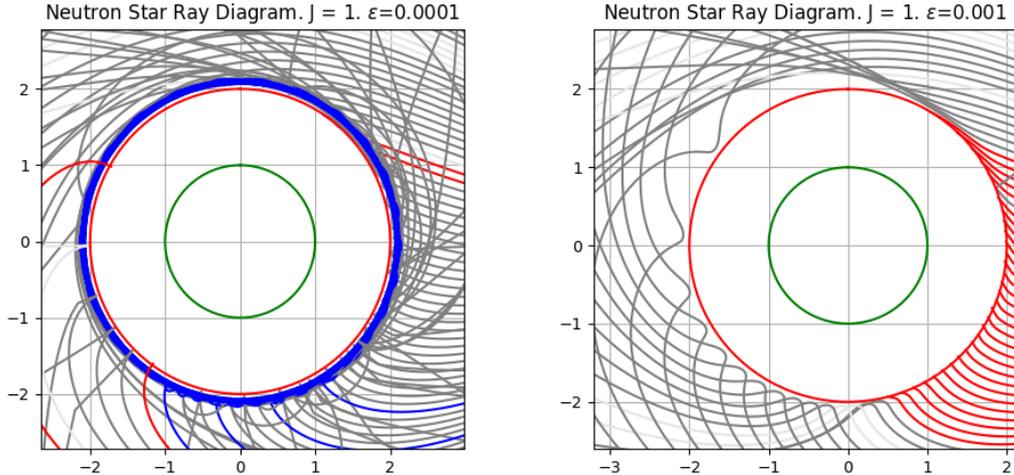
Figure 9: Ray-tracing Glampedakis–Babak neutron star for different values of ϵ. We plot the ergosphere of the underlying Kerr metric. If ray-tracing exceeds 100000 steps the beam is terminated and colored blue, and if the protocol crashes the ray is colored red. We see that any attempt to simulate inside the ergosphere results in a crash. For $\epsilon = 0.0001$ we see strong frame dragging even outside the Kerr ergosphere. For $\epsilon = 0.001$ (and larger) we see rays bouncing off the neutron star.

5.4 Glampedakis–Babak Neutron Star

In this project we study a neutron star metric proposed by Glampedakis and Babak, based on the Kerr metric plus a deviation with scale parameter ϵ. Frame dragging plays a large role in the appearance of the neutron star, but we also discover that beams of light can 'bounce' off the star. These two effects interact and produce a fascinating shadow and gravitational lensing.

As with the Kerr metric, we must decide where to terminate ray-tracing. We use the important surfaces of the Kerr metric as a guideline, but the actual ergosphere and event horizon are likely different. Figure 9 shows that for $\epsilon = 0.0001$ the frame dragging outside the Kerr ergosphere is already very severe, suggesting that the actual ergosphere is larger. This effect diminishes with larger ϵ, causing some rays to enter the Kerr ergosphere. Unfortunately due to singularities in the definition of the Glampedakis–Babak metric, the software immediately crashes (via a logarithm of a negative number). This could possibly be mitigated by choosing a different coordinate system, analogous to the Kruskal–Szekeres coordinates for the black hole. Previous ray-tracing simulations [9] support dynamically changing coordinate systems, but our software does not. Since in the Kerr metric we observed that escape from the ergosphere is unlikely we simply truncate our beams there. This interpretation is also convenient since we can simply assume that the surface of the neutron star must lie within the Kerr ergosphere.

Figure 10 shows the camera images of the spinning neutron star. The shadow is non-spherical and has two notches on either side, reminiscent of the single notch visible for the $J = 1$ Kerr black hole. Furthermore the $\epsilon = 0.01$ neutron stars have small 'wings' that in the $J = 1$ case completely separate from the main shadow. This separation is also visible for the gravitational lensing. All parameters show a sickle on the right which is similar to the Kerr black hole. The $\epsilon = 0.01$ case also shows a small patch on the left side which also appeared in the Kerr black hole. All the neutron stars display a third bright patch, closer to the origin and on the right.

We can explain both the wings and the third patch via the 'bounce' effect. Fig. 11 shows that the $J = 1, \epsilon = 0.01$ neutron star exhibits the same bouncing effect visible in Fig. 9. The gravitational lensing is explained by the light from behind the object bouncing off the surface and into the camera. Frame dragging would usually cause the shadow of the neutron star to be larger, but since much of the light bounces off the surface the star appears smaller. The wings are formed by beams that are too far away to bounce, but close enough to be frame-dragged into the neutron star. The images become more intuitive if one views the region with the lensing patch as a mirage on the shadow of the object.
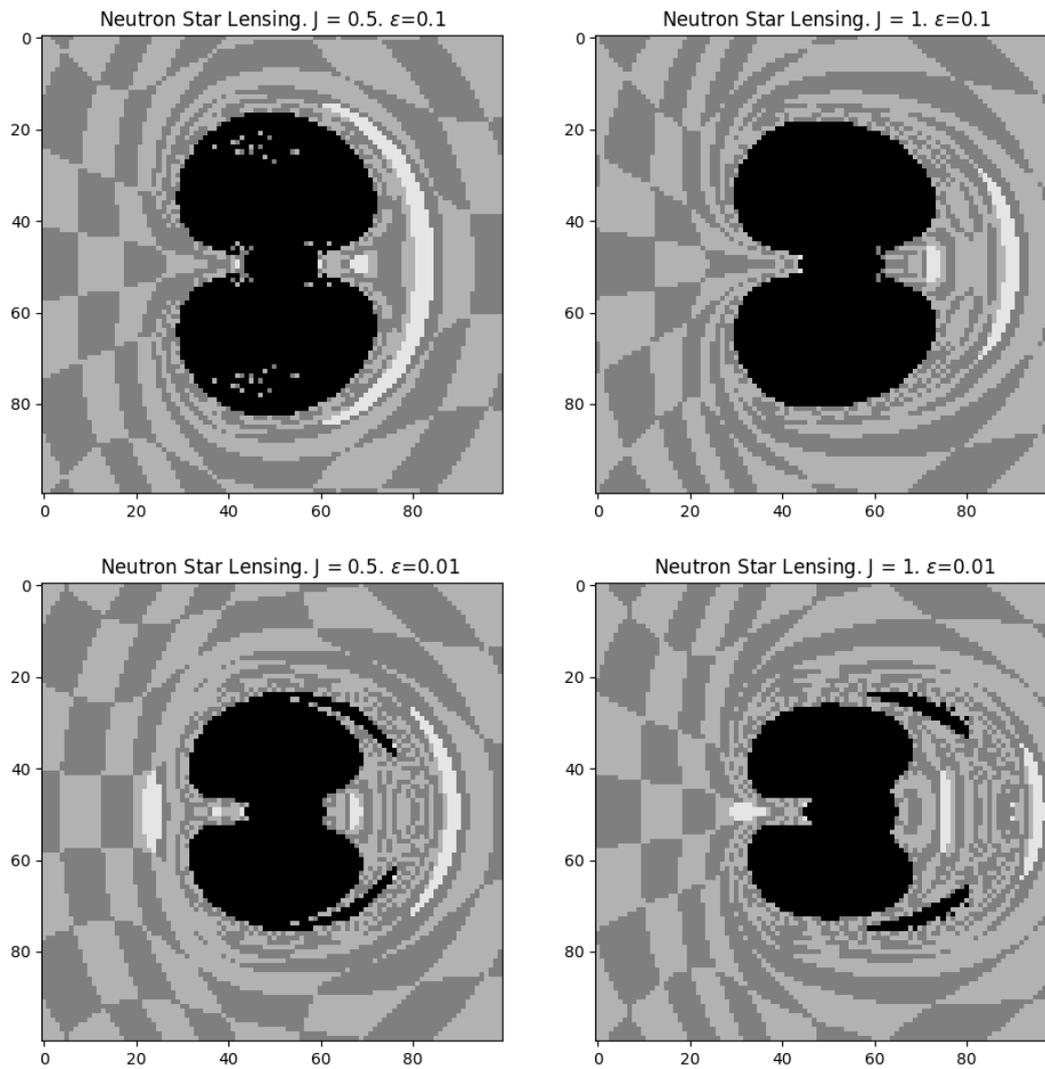
Figure 10: Gravitation lensing with the Glampedakis–Babak neutron star for different values of ϵ and J. The resulting shape is akin to a brain or a Coco de Mer. For $\epsilon = 0.01$ the shadow also has 'wings', as well as strong gravitational lensing causing three images of the bright patch behind the neutron star to be visible. The 'freckles' on $J = 0.5, \epsilon = 0.1$ are most likely numerical artifacts.
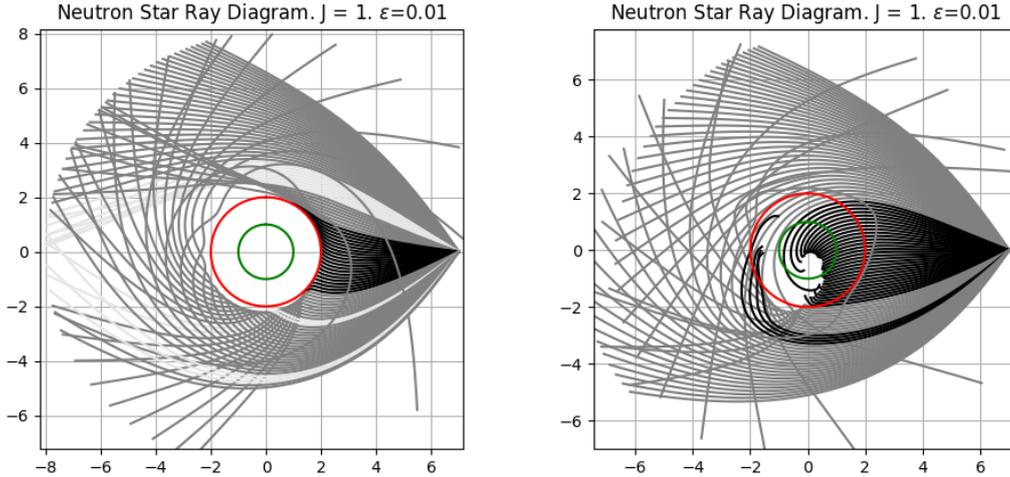
Figure 11: Ray-tracing Glampedakis–Babak neutron star with $J = 1, \epsilon = 0.01$. The left image emits rays in the XY plane, whereas the right image emits the rays at an angle so that the rays correspond to the pixels approximately on line 25 in Fig. 10. The left image explains the third bright patch in the gravitational lensing: some rays bounce off the neutron star. The right image explains the wings: the bounce effect competes with frame dragging causing some inner rays to escape.

6   Conclusions

In this project, we developed Python scripts to perform ray-tracing for a given metric. We organized our scripts to calculate the metric derivatives in a ready-to-use format and to perform ray-tracing using the pre-baked quantities. We tested our code with the Schwarzschild and the Reissner–Nordström metrics. The ray-traced images for the two black holes can be seen in Fig. 5 and 6 respectively. Although, the Schwarzschild and the Reissner–Nordström metrics are interesting solutions of the Field Equations, these metrics are not visually different for photons. Since most neutron stars observed in nature are rotating, we decided to implement the Kerr metric into our program. Visualizations for the Kerr metric are much more interesting and closer to an actual neutron star metric. The Kerr metric plots show the phenomenon of frame dragging in two different ways. In the top-left plot in Fig. 8, one can see photons being preferentially curved under the influence of the rotating spacetime. Fig. 7 shows a zoomed-in view of the ergosphere for two different values of the angular momentum. One can see clearly that increasing the angular momentum increases the volume of the ergosphere. Besides the increase in volume of the ergosphere, one can also notice the more pronounced effect of frame dragging to photon trajectories in the ergosphere. These observations match with the theoretical predictions. However, increasing the angular momentum drastically increases the number of calculations required to ray trace—a challenge not easily overcome in a high-level programming language like Python. A solution to overcome the high volume of calculations was to terminate the integration step in the ray-tracing script to 10000 steps. The upper bound on the integration may add some errors in the plots. A visually interesting effect of frame dragging is the non-spherical appearance of a rotating black hole/neutron star. The deviation from a spherical geometry of the Kerr black hole could be circular orbits of photons which are distorted because of the rotating spacetime.

Since the Glampedakis–Babak metric is an extension to the Kerr metric, we expected some of our results from the Kerr metric to be valid for the neutron star metric as well. Indeed, we could see the ergosphere and frame dragging in our neutron star plots in Fig. 9. The camera images of the neutron star are somewhat analogous to the camera images of the Kerr metric, since the Glampedakis–Babar metric is a quasi-Kerr metric. The differences are caused by a bouncing effect that causes mirages of the sky to appear on the surface of the object.

The work presented in this report shows that even a slow, high-level programming language such as Python can be used to visualize spacetime around massive gravitational bodies with complicated metrics.

References

[1] K. Schwarzschild. Über das Gravitationsfeld eines Massenpunktes nach der Einsteinschen Theorie. *Sitzungsberichte der Königlich Preußischen Akademie der Wissenschaften (Berlin), 1916, Seite 189-196*, 1916.

[2] Roy P. Kerr. Gravitational field of a spinning mass as an example of algebraically special metrics. *Phys. Rev. Lett.*, 11:237–238, Sep 1963.

[3] H. Reissner. Über die Eigengravitation des elektrischen Feldes nach der Einsteinschen Theorie. *Annalen der Physik*, 355:106–120, 1916.

[4] A. Einstein. Über Gravitationswellen. *Sitzungsberichte der Königlich Preußischen Akademie der Wissenschaften (Berlin), Seite 154-167.*, 1918.

[5] Oliver James, Eugénie von Tunzelmann, Paul Franklin, and Kip S Thorne. Gravitational lensing by spinning black holes in astrophysics, and in the movie interstellar. *Classical and Quantum Gravity*, 32(6):065001, 2015.

[6] K. Glampedakis and S. Babak. Mapping spacetimes with LISA: inspiral of a test body in a 'quasi-Kerr' field. *Classical and Quantum Gravity*, 23:4167–4188, June 2006.

[7] F. W. Dyson, A. S. Eddington, and C. Davidson. A Determination of the Deflection of Light by the Sun's Gravitational Field, from Observations Made at the Total Eclipse of May 29, 1919. *Philosophical Transactions of the Royal Society of London Series A*, 220:291–333, 1920.

[8] A. Einstein. Die Grundlage der allgemeinen Relativitätstheorie. *Annalen der Physik*, 354:769–822, 1916.

[9] Corvin Zahn. Vierdimnsionales Ray-tracing in einer gekrümmten Raumzeit. *PhD Thesis, Universität Stuttgart*, January 1991.

[10] Cornelia Vogel. Study of the Hartle-Thorne metric for rotating neutron stars with methods from relativistic visualisation. *Bachelor's Thesis, Universität Stuttgart*, September 2015.

[11] Thomas Muller and Frank Grave. Catalogue of Spacetimes. 2009.

[12] Matt Visser. The kerr spacetime: A brief introduction. *arXiv:0706.0622v3*.

[13] Andreas de Vries. Shadows of rotating black holes approximated by dürer-pascal limaçons. *R. Muno (Hrsg.), Jahresschrift der Bochumer Interdisziplinären Gesellschaft eV 2003, ibidem-Verlag, Stuttgart 2005 (ISBN 3-89821-456-7).*